

Electrostatic Tuning of Spray-Deposited ZnO for Controlled Mobility Enhancement

Andre Zeumault, William Scheideler, and Vivek Subramanian*

Spray-deposited nanocrystalline ZnO films are produced in order to establish empirical relationships between synthetic conditions and the density of states as a means of achieving electrostatic control. By varying the spray-pyrolysis deposition conditions, i.e., substrate temperature, precursor concentration, and flow rate, a wide range of exponentially distributed density of localized states profiles and field-effect mobility values ranging over three orders of magnitude ($0.02\text{--}30\text{ cm}^2\text{ V}^{-1}\text{ s}^{-1}$) are obtained for analysis. It is found that mobility can be controlled by appropriately tuning the shape of the density of states profile, increasing the band tail slope and reducing the band edge concentration of shallow states. Most significantly, it is shown that the shape of the density of states can be modified by adjusting the spray-pyrolysis deposition conditions for electrostatic control. It is found that higher Zn precursor concentration in solution increases the slope of the band tails, leading to higher mobility. Additionally, the band edge concentration is reduced with increased substrate temperature also leading to higher mobility. These results quantify the relationship between defect electrostatics and electron transport while demonstrating electrostatic control via synthetic modification of localized states.

1. Introduction

Large-area, solution-based, roll-to-roll manufacturing techniques are gaining momentum as highly attractive methods for the manufacturing of next-generation materials for displays due to their potential to lower production costs.^[1] Additionally, replacing incumbent amorphous silicon technology with transparent conductive oxides (TCOs) mitigates existing design tradeoffs whereby a transparent thin-film transistor (TFT) permits transistor size optimization without sacrificing brightness due to light absorption/reflection.^[2] Of the various low-cost deposition techniques available for depositing conductive oxides, spray-pyrolysis is particularly interesting, as it combines the synthetic versatility and low-cost benefits of solution-processing with the favorable growth mechanics afforded by an incremental, vapor-like growth process^[3]—typically resulting in films of extraordinary electrical quality. Remarkably, zinc oxide (ZnO) thin films having mobility as high as $85\text{ cm}^2\text{ V}^{-1}\text{ s}^{-1}$ have been integrated into TFTs using spray-pyrolysis on glass,^[4–6] roughly two orders of magnitude higher mobility than existing amorphous silicon technology^[7] and comparable to some of the

best sputtered oxide films.^[8] Additionally, low-voltage inverters have been produced using spray pyrolysis by incorporating self-assembled monolayers as the gate dielectric, further demonstrating applicability for digital logic applications.^[9]

Historically, spray pyrolysis has had the unfortunate drawback of being a blanket film deposition technique, therefore losing its appeal in comparison to the distinct low-cost benefits of purely additive manufacturing techniques such as inkjet-printing.^[10] To address this issue, there have been several successful recent efforts to develop in situ patterning ability of spray-deposited oxide films by exploiting surface-energy differences on substrates to facilitate film growth in targeted hydrophilic regions.^[11–13] Having shown additive process capability, spray-pyrolysis may become a competitive low-cost manufacturing technology for next-generation display materials. However, one

additional drawback yet to be addressed is that TCOs are commonly intrinsically conductive as-deposited. In other words, electrostatics are uncontrolled, inadvertently determined by the synthetic process.^[14]

Intrinsic defects and unintentional doping are presumed to play the dominant role in the observed conductivity of TCOs.^[14] The influence of various intrinsic and extrinsic defects have been studied in detail.^[14,15] However, establishing direct links between conductivity and defect chemistry remains an ongoing experimental challenge, typically requiring more advanced characterization techniques.^[16] This is particularly challenging in thin films fabricated via solution-processing methods due to the parallel processes occurring during synthesis—drying, chemical conversion, film densification, and crystallization.^[17,18] In ZnO and related TCO materials, the general consensus regarding the electron donation and defect compensation mechanism has shifted from one governed by oxygen vacancies to shallow hydrogen electron donors.^[15] For example, recently Siringhaus and co-workers investigated the electronic structure of InZnO films highlighting the importance of hydrogen donor compensation of deep acceptor states by showing negligible changes in oxygen vacancy concentrations despite large differences in electronic conductivity.^[19] However, they note the difficulty in experimentally distinguishing between defects due to variable differences in coordination numbers and bonding character—particularly challenging in disordered thin films. Alternatively, from an electrostatic perspective, the electronic density of states (DOS) can be viewed as a representation of a

Dr. A. Zeumault, W. Scheideler, Prof. V. Subramanian
Department of Electrical Engineering and Computer Sciences
University of California Berkeley
Berkeley, CA 94720, USA
E-mail: viveks@eecs.berkeley.edu

DOI: 10.1002/adfm.201701021

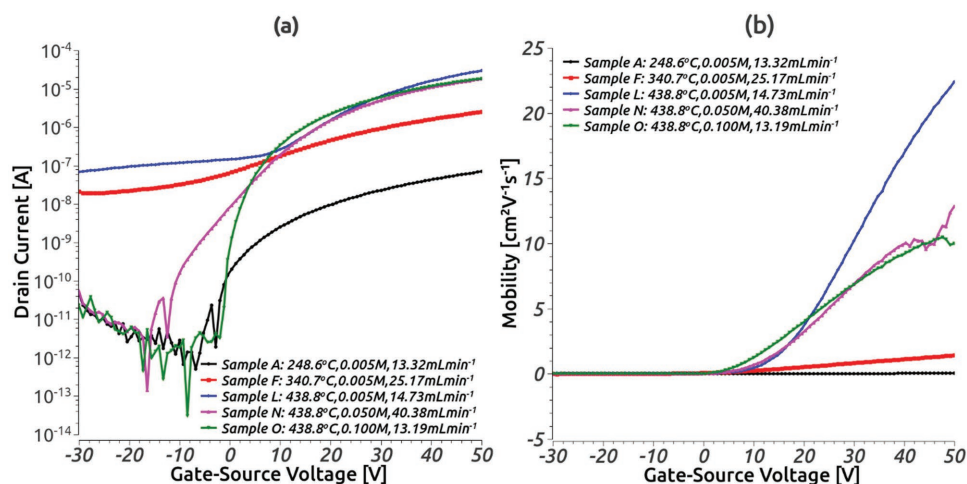


Figure 1. a) Transfer characteristics and b) linear mobility ($V_{DS} = 0.1$ V) for representative devices corresponding to each sample measured in a N_2 environment at room temperature. See Table 1 for thickness and average growth rate for each sample. Data for approximately ten devices per sample are given in the Supporting Information.

particular defect spectrum resulting from a given synthetic condition. As a result, the DOS can be engineered through synthetic conditions—providing a degree of electrostatic control and practical advantage in the absence of knowledge regarding specific defect chemistry.

In this work, we prepare nanocrystalline ZnO films by spray-pyrolysis in order to establish empirical relationships between synthetic conditions and the density of states as a means of achieving electrostatic control. Zinc oxide was selected based on its maturity and established high performance particularly in spray-deposited films.^[4] By virtue of the low carrier densities and small nanometer-sized crystals obtained, grain-boundary barrier heights are determined to be negligibly small, enabling the use of the multiple-trap-and-release (MTR) model for DOS extraction. By varying the spray-pyrolysis deposition conditions—substrate temperature, precursor concentration, and flow rate—we obtain a wide range of exponentially distributed density of states profiles and field-effect mobility values ranging over three orders of magnitude (0.02 – 30 $\text{cm}^2 \text{V}^{-1} \text{s}^{-1}$) for analysis using a simple, custom-built experimental setup. We find that mobility can be controlled by appropriately tuning the shape of the DOS—increasing the band tail slope and reducing the band edge concentration of shallow states. In doing so, we provide additional insight into how electron transport is influenced by the shape of the DOS profiles commonly observed in many TCO materials; this may also be useful for other applications involving these materials such as the electron transport layer in perovskite solar cells.^[20] Most significantly, we show that the shape of the density of states can be modified by adjusting the spray-pyrolysis deposition conditions for electrostatic control. We find that higher Zn precursor concentration in solution increased the slope of the band tails, leading to higher mobility. Additionally, the band edge concentration was reduced with increased substrate temperature also leading to higher mobility.

These results demonstrate that electrostatic control via synthetic modification of the density of states is a potential route to precise design of high-performance conductive oxide

electronics and further underscores the utility of spray-pyrolysis as a technologically viable low-cost manufacturing technique for TCO materials.

2. Results

2.1. Transfer Characteristics, Mobility, and Activation Energy

We begin by evaluating the transfer characteristics and mobility in the linear regime ($V_{DS} = 0.1$ V) for thin film transistors fabricated using each of the synthetic conditions as shown in Figure 1. The specific synthetic conditions corresponding to each sample are labeled as an inset within each figure as an ordered triple—substrate temperature, Zn concentration, and flow rate. The calculated average growth rate (film thickness/deposition time) and the film thickness are shown in Table 1. The synthetic conditions were simultaneously varied over a wide range to produce a variety of different behavior for analysis. To each synthetic condition we assign an identifier—denoted by the letters A, F, L, N, and O—used throughout this work as a reference. For each condition, approximately ten devices were measured and were not found to exhibit significant device-to-device variation in terms of voltage dependence (Figures S1–S5, Supporting Information). As indicated, normal transistor behavior is observed in all cases—withstanding particular differences with regard to specific synthetic conditions. The output characteristics corresponding to each sample are also shown in Figures S6–S10 (Supporting Information). Linear mobility values, extracted using a technique published elsewhere,^[21] are observed to fall within a wide range ≈ 0.02 – 30 $\text{cm}^2 \text{V}^{-1} \text{s}^{-1}$ indicating significant electronic differences, as intended, to be used for further detailed investigation in regard to density of states. This measurement procedure was repeated at different temperatures in the range of 0 – 100 °C in order to obtain activation energy data necessary for density of states extraction. Figure 2 shows the activation energy of mobility as a function of gate–source voltage for each of the

Table 1. Summary of film thickness (t_{FILM}), average growth rate (R_{AVE}), flat-band carrier concentration (N_{FB}), activation energy (E_{A}) XRD (002) peak position (Q_{002}), full-width at half maximum (FWHM), crystal size (L_{C}), and grain boundary barrier heights ($E_{\text{B,calc}}$) computed from Seto's model for each sample assuming a dielectric constant of 10 for ZnO corresponding to the (002) orientation. Broadening factor assumed was 0.9. X-ray wavelength was 1.54056 Å.

Sample	t_{FILM} [nm]	R_{AVE} [nm min ⁻¹]	N_{FB} [cm ⁻³]	E_{A} [eV]	Q_{002} [Å ⁻¹]	FWHM [Å ⁻¹]	L_{C} [nm]	$E_{\text{B,calc}}$ [eV]
A	30	2	1.9×10^{16}	0.173	2.41588	0.08816	7	0.0002
F	106	13.34	1.02×10^{17}	0.130	2.41359	0.03827	15	0.0055
L	90	6.63	1.47×10^{17}	0.088	2.43427	0.03433	17	0.0099
N	38	40.38	8.8×10^{16}	0.305	2.43469	0.04896	12	0.0029
O	20	24.42	9.67×10^{16}	0.717	2.43726	0.06123	10	0.0020

samples. The activation energy decreases monotonically with increasing gate–source voltage, as expected for a trap-limited system. These data were used to extract density of states profiles for each condition. However, as previously mentioned, we must first rule out the possibility of barrier-lowering models providing an alternative explanation for the observed activated behavior.

2.2. Grain-Boundary Barrier Heights

To evaluate the applicability of barrier lowering models, we estimate the barrier heights by evaluating Seto's model commonly applied to polycrystalline semiconductors^[22] (Equation (1)). Binary metal oxides have a tendency to crystallize, unlike their amorphous ternary and quaternary counterparts.^[23–25] As evidenced by **Figure 3**, grazing-incidence X-ray diffraction data indicate that deposited ZnO films are polycrystalline and well matched to the provided powder reference (PDF Card 00-036-1451). As input to the equation for the barrier height corresponding to grain boundaries (Equation (1)), we use crystallite sizes obtained via Scherrer–Debye formula^[26] (Equation (2))

and flat-band electron concentrations obtained from integration of capacitance–voltage data (Equation (3))

$$E_{\text{b}} = \frac{qN_{\text{FB}}L_{\text{C}}^2}{8\epsilon_r\epsilon_0} \quad (1)$$

$$L_{\text{C}} = \frac{0.9\lambda}{\beta\cos\theta} \quad (2)$$

$$N_{\text{FB}} = \frac{1}{qt_{\text{film}}} \int_{v_{\text{min}}}^{V_{\text{FB}}} C(V_{\text{gs}})dV_{\text{gs}} \quad (3)$$

An upper bound for the estimation of the grain boundary barrier height is obtained using the full-width at half maximum (FWHM) of the narrowest peak, corresponding to the largest crystallites present in the film. A summary of the data relevant for determining crystallite size estimates and barrier heights is given in Table 1, corresponding to the most prominent (002) crystal orientation. To convert areal charge density (obtained from capacitance) to volumetric charge density, we assume the accumulation charge to be uniformly distributed throughout the film thickness. This assumption is justified by

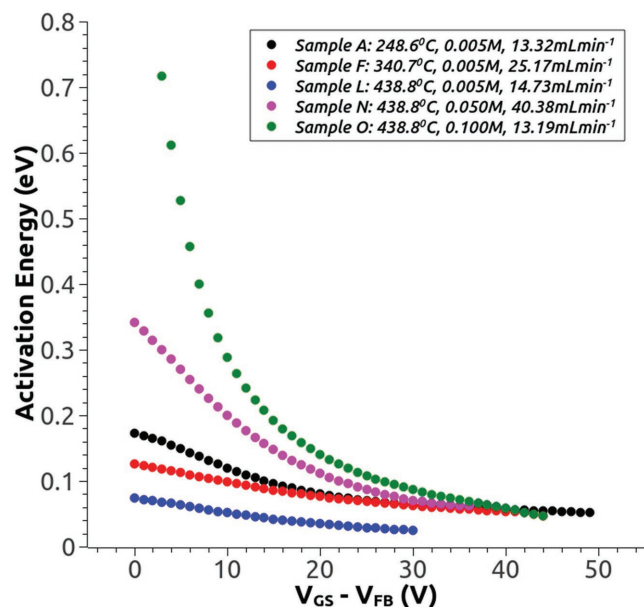


Figure 2. Activation energy as a function of gate–source voltage above flat-band for each sample condition.

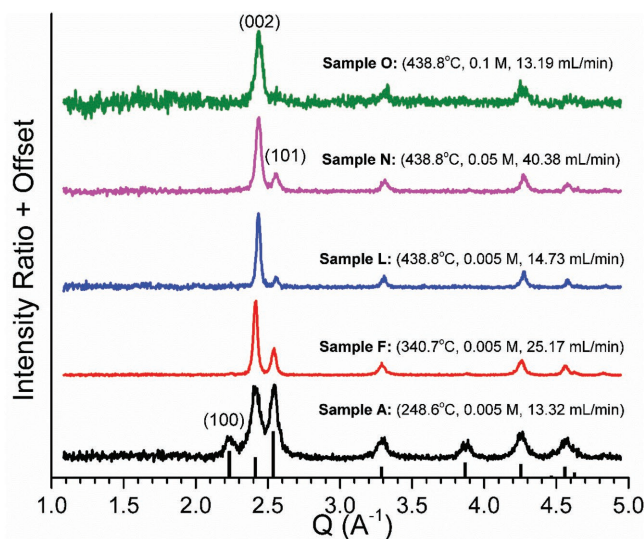


Figure 3. (Top) Grazing incidence X-ray diffraction data for each sample condition. Reference data shown corresponding to PDF Card 00-036-1451.

the large Debye lengths (λ_D) and small film thicknesses (t_{film}) in these materials—such that $\lambda_D \gg t_{\text{film}}$ —resulting in a fully accumulated film at flat band.^[27] Additionally, the carrier density is extracted at flat band such that there is no band bending in the ZnO—further justifying the assumption of a spatially uniform charge density. Using these data as input, in all cases, the grain boundary barrier heights are calculated to be significantly below the thermal energy at room temperature (≈ 0.026 eV) and therefore negligibly small. Such small barriers to conduction are inconsistent with relatively large measured activation energies of mobility (0.088–0.717 eV; Table 1) and therefore do not provide a physically consistent alternative interpretation. This allows us to justifiably neglect barrier-lowering models and percolation and, instead, apply the more appropriate MTR model for interpreting the activation energy of mobility when deriving density of states. We note however that although barrier-lowering models do not allow for accurate interpretation of activation energy, the formation of large grains and smooth surfaces has been shown to lead to higher mobility films for the same zinc acetate chemistry.^[28]

2.3. Density of States

The experimental techniques used to extract density of states profiles in disordered semiconductors are largely based on the interpretation of activation energies obtained from mobility measurements—assuming a particular transport mechanism. The models used to describe activated conduction in disordered solids are a combination of percolation conduction, hopping, barrier-lowering models, and multiple-trap-and-release (or trap-limited conduction).^[29] A good illustration depicting these various mechanisms is provided in Lee et al.^[30] Percolation conduction has been applied to nanocrystalline ZnO films to explain the onset of conduction (i.e., turn-on voltage) for a single midgap defect state.^[31] In this model, site occupation probability is equated to the relative fraction of free carriers whereas bond formation probability is given by a Boltzmann factor due to thermionic emission over grain boundary potential barriers. Physically speaking, the latter assumption is identical to that of barrier lowering models that we have specifically addressed in the previous section. More commonly, percolation conduction is typically applied to ternary and quaternary compounds such as InGaZnO in the large gate–source voltage limit, in which percolation has been suggested due to random compositional disorder of cationic species comprising the conduction band.^[32] However, recently it was shown that the apparent electron delocalization in InGaZnO is an artifact of the insufficiently sized simulation domains typically used in periodic band-structure calculations, and above-threshold percolation conduction may be unphysical.^[33] Hopping conduction is present in sufficiently disordered materials, although tends to be practically significant at low temperatures.^[34] At higher temperatures, phonon absorption easily liberates localized electrons into extended states, so that, by comparison, hopping events contribute negligibly to the overall conductivity. Therefore, at sufficient temperatures, hopping conduction can be reasonably neglected, and binary conductive oxides (e.g., ZnO, SnO₂, and In₂O₃) are expected to exhibit either a barrier-lowering or MTR mechanism. In the previous section, barrier-lowering models

were found to be inconsistent with measured activation energies suggesting that the MTR model is more appropriate in the present case.

Following the assumptions of the MTR model, as is customarily done in the literature regarding TCO TFTs,^[35] we assume that trap states below the Fermi energy make negligible contributions to the measured mobility. In other words, we ignore hopping conduction between them—a reasonable approximation at the sufficiently high temperatures used in this work (0–100 °C). Since mobility in purely hopping based systems tends to be low (< 1 cm² V⁻¹ s⁻¹), this assumption is further justified by the relatively high mobility typically observed in TCOs (10–100 cm² V⁻¹ s⁻¹) and also in this work. Alternatively, we assume that mobility is limited by thermal excitation of trapped electrons distributed below the Fermi energy to the conduction band. This provides a convenient interpretation of the activation energy as the trap depth below the conduction band edge ($E_A = E_C - E_T$). Since the accumulation charge in the semiconductor is known self-consistently from integration of capacitance–voltage data, this produces a charge versus trap depth curve, which we subsequently fit to an assumed exponential distribution. The exponential distribution is characterized by two parameters—band edge concentration (N_0) and band tail slope (E_0)—and is a commonly used representation of the density of states for these materials^[35,36] (Equation (4)). These assumptions form the basis for the commonly used multiple-trap-and-release model for mobility and are the foundation of the technique used to quantify the density of states profiles for each synthetic condition.^[35]

$$N(E) = N_0 e^{\frac{E-E_c}{E_0}} \quad (4)$$

Density of states profiles for each condition were extracted based on the above assumptions. As shown in **Figure 4a**, the different synthetic conditions produce a wide range of DOS profiles for analysis. These concentrations are reasonable when compared to other reports in the literature for ZnO.^[35] For reference, we also plot the theoretical free electron concentration for a bulk semiconductor using an effective conduction band density of states of 4×10^{18} cm⁻³. The shape of the density of states profile can be generalized to an exponential distribution—parameterized into an energy slope parameter and concentration at the band edge according to Equation (4). A statistical summary of the mobility values corresponding to these conditions is provided in **Figure 4b** in which differences between samples can be seen to originate from the differences in density of states produced by varying synthetic conditions. When drawing conclusions from density of states extracted using this technique, it is important to note that both the contact resistance and film thickness may affect the activation energy. Torricelli et al. have measured the activation energy of mobility as a function of gate–source voltage for devices having different channel lengths.^[37] They show a difference in activation energy between devices having channel lengths of 40 and 10 μm of ≈ 30 meV, despite the use of Schottky gold contacts for the source/drain. In this work, we have used 20 μm channel lengths, and Ohmic aluminum contacts for all samples previously shown to exhibit negligible contact resistance of

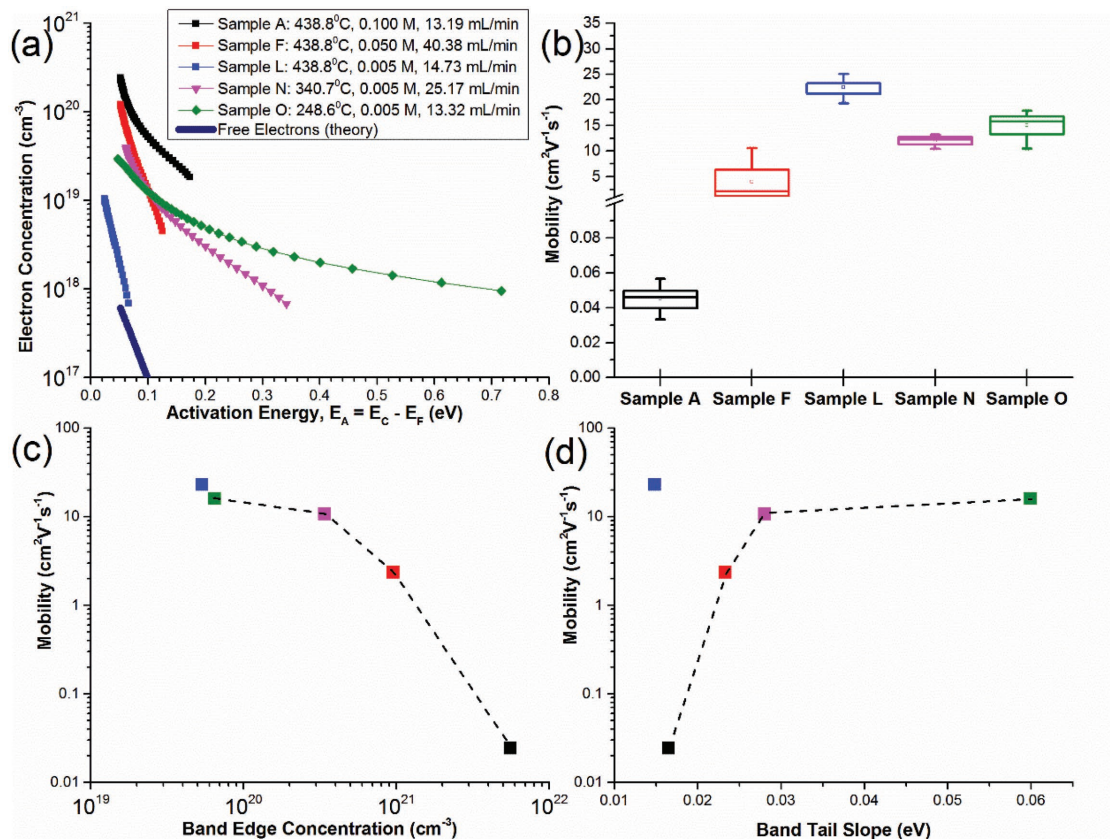


Figure 4. a) Extracted localized carrier concentrations as a function of energy below the conduction band edge. b) Box-and-whisker plot summary of mobility for the various sample conditions investigated. c) Mobility as a function of extracted band tail concentration. d) Mobility as a function of extracted band tail slope.

$4 \Omega \text{ cm}$.^[38] Therefore, we do not expect a significant influence on the measured DOS due to contact resistance.

We evaluate the effect of film thickness shown in Figure S11 (Supporting Information) for two identically processed ZnO films having a thickness of 20 and 85 nm. As shown, the maximum activation energy is higher in the 20 nm film than in the 85 nm film. Furthermore, the minimum activation energy and gate-voltage dependence converges for the two devices as the gate-voltage is increased. As expected, the thicker film has more bulk conduction than the thin film, resulting in a perceived lower peak activation energy for field-effect mobility. This can lead to mobility overestimation and has been demonstrated in the literature.^[39] To avoid erroneous interpretation of activation energy, in the subsequent analysis, we focus on the shallow (i.e., low energy) region of the DOS to evaluate the effects of synthetic conditions.

In order to establish a general understanding as to how the specific shape of the DOS affects electron transport, we evaluate the mobility as a function of the band edge concentration (N_0) and band tail slope (E_0) as shown in Figure 4c,d. We find that the mobility is a strong function of the shape of the density of states profile, exhibiting sensitivity to both the band tail slope and band edge concentration. Evidently, as the band edge concentration is increased, the mobility reduces, dropping off rapidly at values exceeding $\approx 10^{21} \text{ cm}^{-3}$. Furthermore, as the band tail slope increases, mobility is found to increase. Interestingly, the greatest change in mobility occurs as the band

tail slope approaches the thermal energy ($\approx 0.026 \text{ eV}$), below which the mobility is greatly deteriorated. For the applicability of this analysis, it is assumed that free electron concentrations are much smaller than trap states (i.e., trap-limited conduction). We note that the data point not included in the interpolations in Figure 4c,d corresponds to the highest mobility sample (Sample L) which falls outside of the scope of the MTR treatment due to its relatively low trap concentration—as can be seen in Figure 4a. For the remaining conditions, however, localized electrons clearly outnumber free electrons, so that the assumptions of trap-limited conduction are valid. We illustrate this point more clearly by evaluating the ratio of free charge to total charge against gate-source voltage (Figure S12a, Supporting Information) as well as mobility against the ratio of free charge to total charge (Figure S12b, Supporting Information). It can be seen that, for Sample L, the fraction of free carriers varies between 34% and 14% as the gate-source voltage is increased. This is a significant fraction of the total charge such that the assumptions of trap-limited conduction may no longer hold (Figure 4d). For the remaining samples however, the fraction of free carriers is below 3% such that the trap-limited conduction assumptions are appropriate.

Having shown how the shape of the DOS profiles affects mobility, we now show how the DOS profiles are modified by synthetic conditions—substrate temperature, Zn concentration, and flow rate. For completeness, scatter plots corresponding

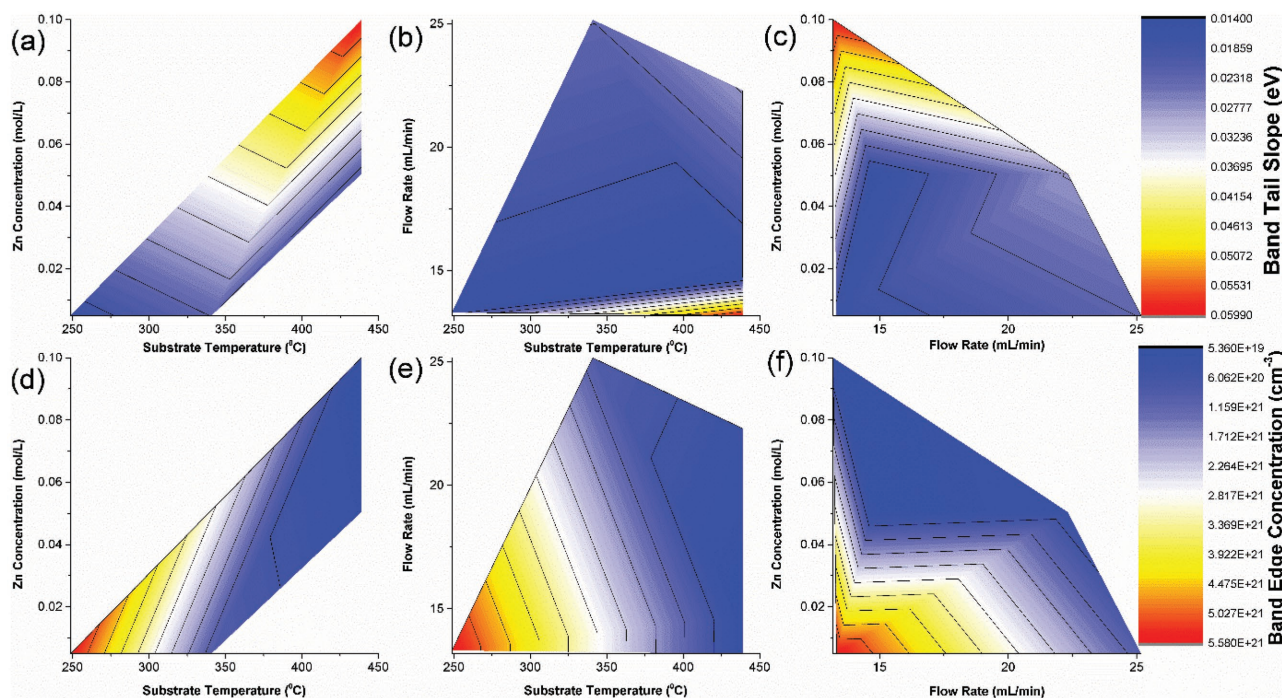


Figure 5. a–c) Contour plots of band tail slope, and d–f) band edge concentration as a function of spray deposition parameters.

to the data are given in Figure S13 (Supporting Information), though the data are best visualized as a 3D contour plot (Figure 5). By inspection of Figure S13 (Supporting Information), substrate temperature and Zn concentration have the strongest effects. It is immediately evident that increasing substrate temperature reduces the band edge concentration (Figure S13a, Supporting Information) and increasing the Zn concentration increases the band tail slope (Figure S13e, Supporting Information)—both actions leading to higher mobility. Trends with flow rate are much subtler, due to the overwhelmingly strong effects of substrate temperature and concentration. To better illustrate the correlated nature of the effects of the various synthetic conditions, in Figure 5 we depict the same data as a series of contour plots corresponding to all possible parameter pairs. Contour plots corresponding to band tail slope are shown in Figure 5a–c, while those corresponding to band edge concentration are shown in Figure 5d–f. Here, the strong effects of substrate temperature and Zn concentration are clearly indicated. In general, increasing substrate temperature and Zn concentration is beneficial in increasing band tail slope and reducing band edge concentration—thereby increasing mobility. Therefore, we reiterate that in regard to synthetically tuning the density of states profiles so as to maximize mobility, it is necessary to increase the band tail slope and reduce the band edge concentration achieved by adjustment of two deposition parameters—Zn concentration and substrate temperature.

3. Discussion

3.1. General Transport Behavior

The general dependence of mobility on the density of states profile can be explained using Fermi–Dirac statistics, offering

additional insight into electronic transport in systems having exponentially distributed band tails. As the Fermi energy moves closer toward the conduction band edge, more electrons are promoted both into free states and localized states. This follows from the fact that the density of localized states increases toward the conduction band edge (Figure 4a). The rate of population of free states is fixed and determined by the thermal energy (i.e., Boltzmann statistics), whereas the rate of population of localized states is variable depending on the band tail slope. When the band tail slope becomes less than the thermal energy, a greater proportion of induced electrons are expected to occupy localized states than free states upon increasing the Fermi energy toward the conduction band edge. These localized states correspond to ionized acceptors^[35] and are therefore expected to scatter free electrons as they become occupied. Therefore, when the Fermi energy enters these shallow states (corresponding to high gate–source voltages) such that activation energies become small and sufficient carriers thermally excite into the conduction band, transport may become limited by impurity scattering rather than availability of carriers. In other words, in addition to the benefit gained by having more electrons in free states, there is a proportional increase in ionized impurity scattering, potentially limiting systems having band tail slope below the thermal energy.

Based on the implications of these new results, it is worthwhile to compare to recent work, in which we showed how defective dielectrics can imitate the role of electron donors in ZnO by compensating deep acceptor states, raising the Fermi energy thereby increasing the number of free electrons available for conduction.^[38] This explanation builds on the general consensus in the field regarding how compensation improves mobility—either through shallow donors or by electron transfer at interfaces. By comparison to this work,

evidently, the effectiveness of donor compensation methods for improving mobility may be reduced by sufficiently small band tail slopes, whereby compensation alone may not be sufficient in overcoming the scattering ability of ionized acceptor states. By extension, this may help to explain why different dielectrics show a more pronounced mobility enhancement than others when paired with TCOs—potentially resulting in different DOS profiles (e.g., different band tail slopes) due to interactions with the dielectric during growth.

Notwithstanding its practical utility, the unfortunate drawback of this method in using synthetic conditions to modify the DOS is that the underlying mechanism responsible for the electronic changes is unknown. In the next section, we attempt to gain further insight regarding the mechanism(s) by evaluating the extent of film crystallinity and hydroxide content—both known to have strong effects on mobility.

3.2. Relation of Mobility to Film Orientation and Hydroxide Content

Film orientation and hydroxide content are two of the most important factors known to impact the electron mobility in ZnO thin films. Evidently, as-deposited ZnO thin films tend to be polycrystalline, having a mobility which is strongly dependent on film orientation—exhibiting the maximum mobility for *c*-axis (002) oriented films.^[23] Consequently, there is a wealth of data showing reduction in mobility due to reduction of texture in ZnO. Likewise, mobility has also been shown to be negatively correlated to hydroxide content.^[40] This is a rather ubiquitous observation across metal oxides in general (e.g., SnO₂, In₂O₃, and ZnO to name a few), and is particularly problematic when low processing temperatures are used. Zinc acetate dehydrate decomposes to oxide and/or hydroxide species between 190 and 310 °C.^[41] Marks and co-workers showed that InZnO films annealed below 300 °C were almost exclusively composed of metal-hydroxide species rather than desired metal-oxide species.^[42] At higher processing temperatures, conversion to the oxide may be nonlimiting, and mobility may show a weaker dependence upon hydroxide content. For example, Cho and co-workers showed a relatively insensitive field-effect mobility to the presence of the high energy peak associated with hydroxide or loosely bound oxygen.^[43] Other factors such as porosity, residual carbon, and/or counter ions are also important but none have been shown to impact mobility as strongly as do film orientation and hydroxide content. Therefore, we evaluate our observations of mobility within the context of hydroxide content and film orientation, in an attempt to gain further insight regarding the changes in density of states.

As shown in **Figure 6a**, ZnO films have noticeably different orientations, depending on the synthetic conditions. In **Figure 6b**, we evaluate the effect of this orientation dependence on mobility by plotting mobility versus the ratio of the integrated area of the (101) and (002) peaks. As expected, mobility increases strongly as the films become increasingly oriented along the (002) direction. In **Figure S14** (Supporting Information), scanning electron microscopy (SEM) images indicate a rough surface topology consisting of grains protruding at different angles. This occurs due to the columnar-like growth of

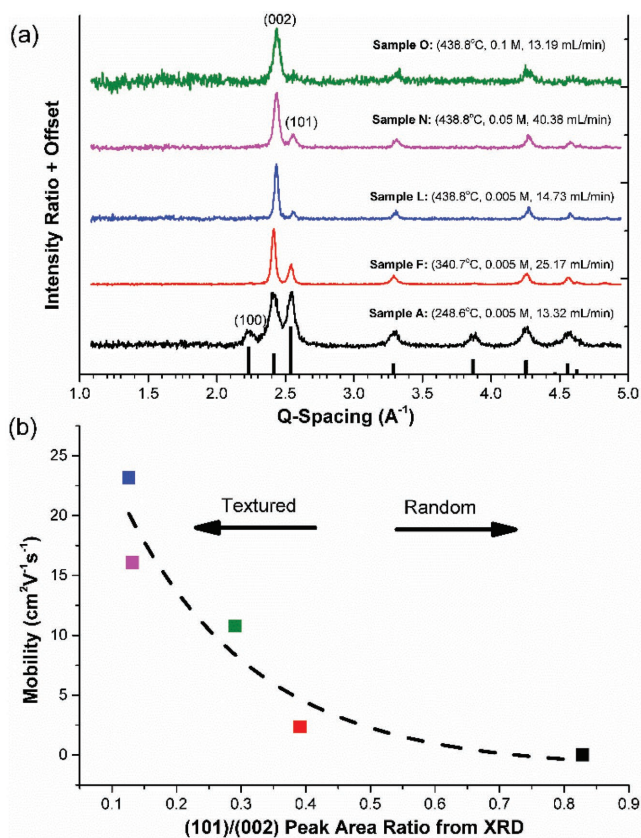


Figure 6. a) Grazing-incidence X-ray diffraction (GIXD) data and b) linear mobility as a function of (101)/(002) ratio of integrated peak areas.

hexagonal ZnO grains^[44] and is essentially a visible representation of the observation of different orientations observed in the diffraction pattern. We further investigate the surface morphology via atomic force microscopy (AFM) measurements as shown in **Figures S15–S19** (Supporting Information). A summary of average roughness, rms roughness, and average grain size is given in **Table S1** (Supporting Information). Grain sizes are found to be consistent with SEM and are noticeably larger than the crystal sizes determined by X-ray diffraction (XRD), suggesting that the majority of the grain is noncrystalline and consistent with the assumption of trap-limited conduction. High-resolution TEM studies of grain boundaries in ZnO indicate different atomic structures at grain boundaries depending on the degree of mismatch between lattice planes.^[45] Therefore, it is plausible that the DOS modification we achieve by adjusting synthesis conditions originates due to the behavior of grain boundary defects affected by differences in film orientation.

The chemical composition of the films was assessed via X-ray photoelectron spectroscopy (XPS) by comparing the O(1s) core states as shown in **Figure 7**. As is customarily done in the literature, we separate the total O(1s) peak into two peaks, assigning the higher energy peak to hydroxide and the lower energy peak to metal oxide. It is also common to include a third peak having binding energy between the hydroxide and oxide components, which is believed to be due to oxygen vacancies;^[46] however, we were able to obtain reasonably good fits to the data by using just the aforementioned two peaks. Mobility was plotted as a

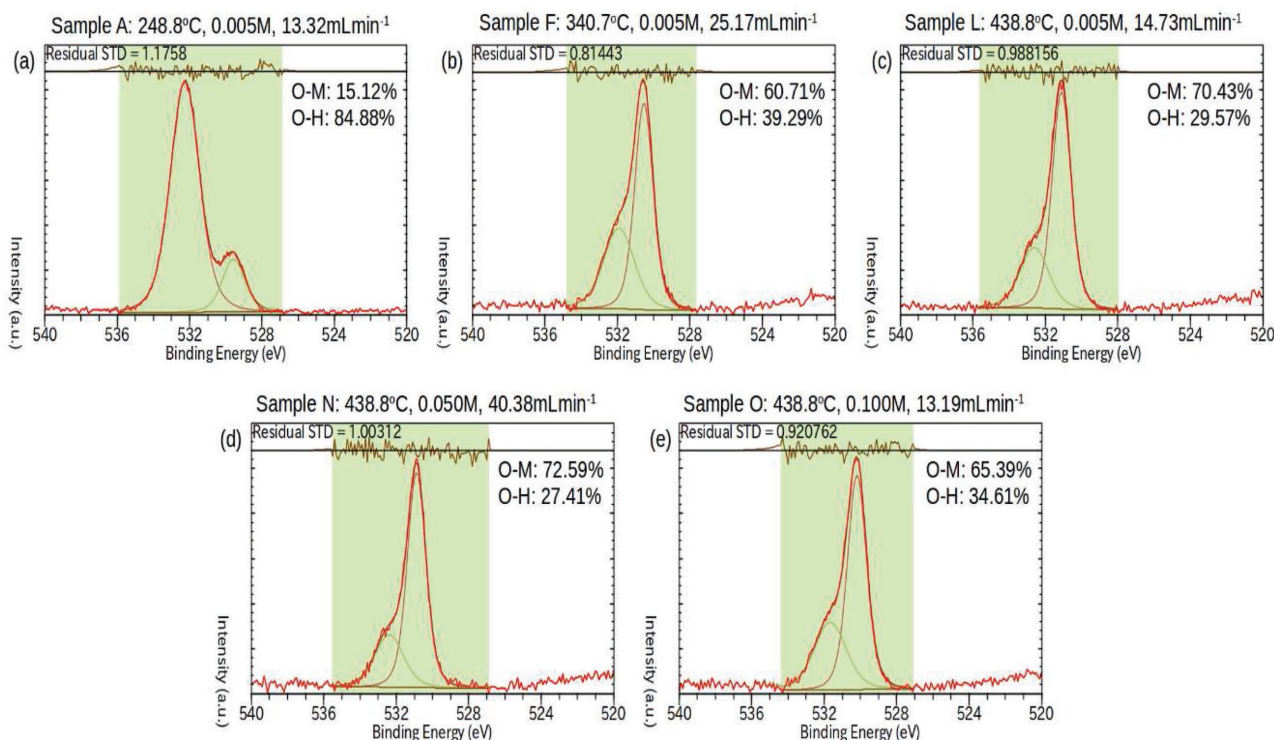


Figure 7. X-ray photoelectron spectroscopy results of the oxygen 1s peak for a) Sample A, b) Sample F, c) Sample L, d) Sample N, and e) Sample O. In each case, the raw data are shown in red. Fits for the metal-oxide (O-M) and hydroxide (O-H) contributions are also shown in green and brown along with the resulting estimated contributions from each species by percentage area.

function of hydroxide content ($O_{OH}(1s)/O_{total}(1s)$) to evaluate the impact of conversion on transport in **Figure 8a**. We find that as the hydroxide content increases, mobility reduces, as is commonly observed in the literature.^[47] Again, we evaluate these correlated effects on a contour plot to attempt to separate the main effects (**Figure 8b**). As shown, both hydroxide content and orientation have strong effects on mobility—showing mobility enhancement with reduced hydroxide content and increased (002) texturing. As a result, we cannot determine which effect dominates in this particular case.

4. Conclusion

In summary, we have demonstrated a simple means of electrostatic control in zinc oxide thin-film transistors by showing how the synthetic conditions of spray pyrolysis—substrate temperature, precursor concentration, and flow rate—can be adjusted to modify the electronic density of states profiles, thus providing electrostatic control. By approximating the defect spectrum as an exponential distribution, we parameterize the density of states into two components—band edge concentration and band tail slope—and have shown how to modify these independently to adjust film properties for higher mobility. We find that increasing substrate temperature results in significant reduction in band edge concentration while increasing Zn concentration increases the band tail slope—both of which resulted in higher mobility. Investigation of film crystalline orientation and hydroxide content shows that both are significant factors in

determining mobility, although unfortunately we were unable to clearly isolate the dominant effect. Most importantly, however, this work shows that the defect spectrum (i.e., electrostatics) in ZnO is synthetically tunable and can be made to achieve a particular electrostatic behavior for transistor applications. Furthermore, since the analysis is based on widespread observation of exponentially distributed density of states profiles common to several TCO materials, it may be possible to modify the electrostatics of other semiconducting TCOs (e.g., In_2O_3 , $InGaZnO$, $InZnO$, $ZnSnO$, etc.) using this same strategy as well. Having provided a simple means to address the practical issue regarding the lack of electrostatic control in TCO based TFTs, the utility of spray-pyrolysis as a viable, low-cost manufacturing technique for future displays becomes more readily apparent.

5. Experimental Section

ZnO Precursor Solution: The ZnO precursor solution consisted of zinc acetate (Aldrich 383317) dissolved in methanol at various concentrations (0.005–0.1 M).

ZnO Thin-Film Preparation: Semiconducting ZnO thin films were prepared using a spray pyrolysis technique. The precursor solution was sprayed onto heavily doped n-type silicon wafers prefixed as having 100 nm of thermally grown SiO_2 that served as the gate dielectric. These substrates were placed on a hotplate (250–450 °C) at a stationary fixed nozzle-to-substrate distance of 14 inch. using compressed air at 20 psi and the precursor solution was directed onto the substrates at various flow rates (1–20 mL min⁻¹). Deposition times varied from 1 to 15 min.

Metallization and Lithography: Aluminum (100 nm thick) was thermally evaporated (1–2 × 10⁻⁶ Torr) to serve as source/drain

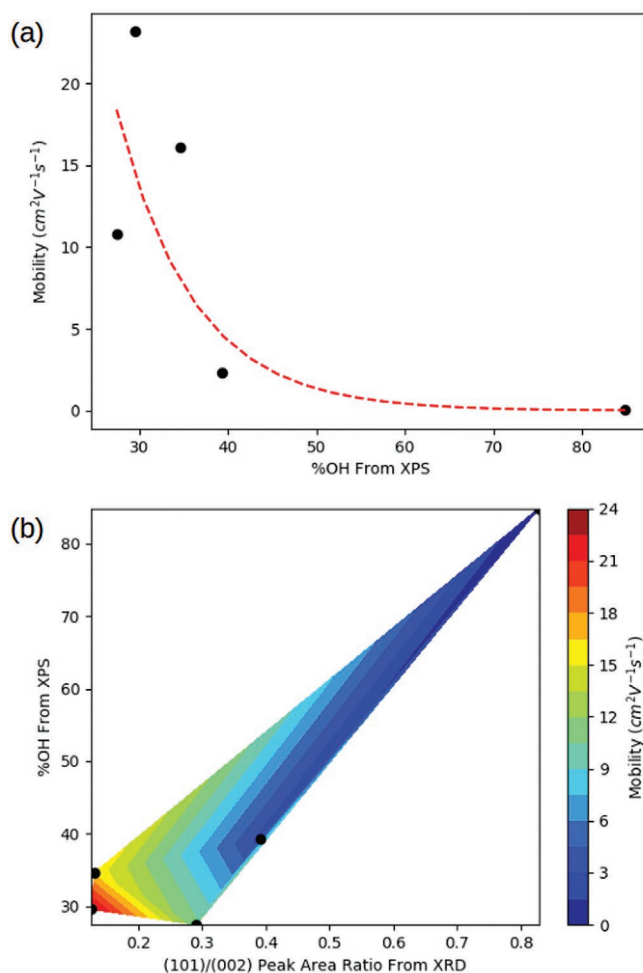


Figure 8. a) Mobility as a function of hydroxide content. b) Contour plot of mobility versus hydroxide content and extent of texture, as indicated by %OH obtained from O(1s) peak analysis and integrated peak ratios (101)/(002) from GIXD, respectively.

electrodes. ZnO was patterned using standard I-line photolithography and etched in aqueous hydrochloric acid (1:500 HCl:H₂O).

Electrical Characterization: Long channel devices (channel length/width = 200 μm/20 μm) were measured using an HP4155C semiconductor parameter analyzer under medium integration time. All mobility measurements were performed in the linear region ($V_{DS} < 100$ mV) according to an improved combined capacitance/conductance (C-V/G-V) technique reported in detail elsewhere.^[21] Density of states profiles were extracted using temperature-dependent mobility measurements in the temperature range of 0–100 °C in a nitrogen environment. Nitrogen was used as an ambient to reduce moisture absorption on the exposed back surfaces of the ZnO films.

Morphological Characterization: Film thickness was characterized using a Dektak profilometer. The chemical composition of the deposited films was evaluated using XPS on a PHI 5000 VersaProbe. The crystallinity of the deposited films was determined using X-ray diffraction on a PANalytical X'PERT system in grazing-incidence mode at 0.14° with a Cu K-α source having a wavelength of 1.54056 Å. SEM images were obtained using an FEI Quanta 3D FEG system. Atomic force microscopy was performed using an NT-MDT system using an HQ:NSC35/Pt 150-300 kHz 5.4–16 N m⁻¹ tip. Gwyddion was used to perform roughness and grain-size analysis.

Supporting Information

Supporting Information is available from the Wiley Online Library or from the author.

Acknowledgements

This work was funded in part by the Semiconductor Research Corporation and the BASF California Research Alliance. The authors would also like to thank Gerd Grau for assisting them with SEM measurements and Steve Volkman and Jeremy Smith for helpful theoretical discussions.

Conflict of Interest

The authors declare no conflict of interest.

Keywords

defects, displays, large-area electronics, sol-gels, transport

Received: February 23, 2017

Revised: April 27, 2017

Published online: June 30, 2017

- [1] V. Subramanian, J. B. Chang, A. d I F. Vornbrock, D. C. Huang, L. Jagannathan, F. Liao, B. Mattis, S. Molesa, D. R. Redinger, D. Soltman, S. K. Volkman, Q. Zhang, in *Solid-State Device Research Conf. 2008 ESSDERC 2008 38th European*, **2008**, pp. 17–24.
- [2] R. M. Pasquarelli, D. S. Ginley, R. O'Hayre, *Chem. Soc. Rev.* **2011**, *40*, 5406.
- [3] L. Filipovic, S. Selberherr, S. Selberherr, G. Mutinati, E. Brunet, S. Steinhauer, A. Kock, J. Teva, J. Kraft, F. Schrank, *Proc. World Congr. Eng.*, **2013**, pp. 987–992.
- [4] G. Adamopoulos, S. Thomas, P. H. Wöbkenberg, D. D. C. Bradley, M. A. McLachlan, T. D. Anthopoulos, *Adv. Mater.* **2011**, *23*, 1894.
- [5] G. Adamopoulos, A. Bashir, S. Thomas, W. P. Gillin, S. Georgakopoulos, M. Shkunov, M. A. Baklar, N. Stingelin, R. C. Maher, L. F. Cohen, D. D. C. Bradley, T. D. Anthopoulos, *Adv. Mater.* **2010**, *22*, 4764.
- [6] X. Yu, J. Smith, N. Zhou, L. Zeng, P. Guo, Y. Xia, A. Alvarez, S. Aghion, H. Lin, J. Yu, R. P. H. Chang, M. J. Bedzyk, R. Ferragut, T. J. Marks, A. Facchetti, *Proc. Natl. Acad. Sci. USA* **2015**, *112*, 3217.
- [7] P. G. Le Comber, W. E. Spear, *Phys. Rev. Lett.* **1970**, *25*, 509.
- [8] C. Brox-Nilsen, J. Jin, Y. Luo, P. Bao, A. M. Song, *IEEE Trans. Electron Devices* **2013**, *60*, 3424.
- [9] A. Bashir, P. H. Wöbkenberg, J. Smith, J. M. Ball, G. Adamopoulos, D. D. C. Bradley, T. D. Anthopoulos, *Adv. Mater.* **2009**, *21*, 2226.
- [10] P. Calvert, *Chem. Mater.* **2001**, *13*, 3299.
- [11] A. Zeumault, W. Scheideler, G. Grau, J. Smith, V. Subramanian, *Adv. Electron. Mater.* **2016**, *2*, 1500326.
- [12] H. Faber, B. Butz, C. Dieker, E. Spiecker, M. Halik, *Adv. Funct. Mater.* **2013**, *23*, 2828.
- [13] B. Wang, X. Yu, P. Guo, W. Huang, L. Zeng, N. Zhou, L. Chi, M. J. Bedzyk, R. P. H. Chang, T. J. Marks, A. Facchetti, *Adv. Electron. Mater.* **2016**, *2*, 1500427.
- [14] M. D. McCluskey, S. J. Jokela, *J. Appl. Phys.* **2009**, *106*, 071101.
- [15] C. G. Van de Walle, *Phys. Rev. Lett.* **2000**, *85*, 1012.
- [16] F. Tuomisto, V. Ranki, K. Saarinen, D. C. Look, *Phys. Rev. Lett.* **2003**, *91*, 205502.
- [17] L. L. Hench, J. K. West, *Chem. Rev.* **1990**, *90*, 33.

- [18] C. J. Brinker, G. W. Scherer, *Sol-Gel Science: The Physics and Chemistry of Sol-Gel Processing*, Academic Press, UK **2013**.
- [19] J. Socratous, K. K. Banger, Y. Vaynzof, A. Sadhanala, A. D. Brown, A. Sepe, U. Steiner, H. Siringhaus, *Adv. Funct. Mater.* **2015**, *25*, 1873.
- [20] J. H. Heo, M. H. Lee, H. J. Han, B. R. Patil, J. S. Yu, S. H. Im, *J. Mater. Chem. A* **2016**, *4*, 1572.
- [21] A. Zeumault, V. Subramanian, *IEEE Trans. Electron Devices* **2015**, *62*, 855.
- [22] J. Y. W. Seto, *J. Appl. Phys.* **1975**, *46*, 5247.
- [23] S. Fujihara, C. Sasaki, T. Kimura, *Appl. Surf. Sci.* **2001**, *180*, 341.
- [24] T. Fukano, T. Motohiro, *Sol. Energy Mater. Sol. Cells* **2004**, *82*, 567.
- [25] O. Dobrozhan, A. Opanasyuk, M. Kolesnyk, M. Demydenko, H. Cheong, *Phys. Status Solidi A* **2015**, *12*, 2915.
- [26] A. L. Patterson, *Phys. Rev.* **1939**, *56*, 978.
- [27] R. L. Hoffman, *J. Appl. Phys.* **2004**, *95*, 5813.
- [28] G. Adamopoulos, A. Bashir, W. P. Gillin, S. Georgakopoulos, M. Shkunov, M. A. Baklar, N. Stingelin, D. D. C. Bradley, T. D. Anthopoulos, *Adv. Funct. Mater.* **2011**, *21*, 525.
- [29] S. Lee, K. Ghaffarzadeh, A. Nathan, J. Robertson, S. Jeon, C. Kim, I.-H. Song, U.-I. Chung, *Appl. Phys. Lett.* **2011**, *98*, 203508.
- [30] S. Lee, A. Nathan, Y. Ye, Y. Guo, J. Robertson, *Sci. Rep.* **2015**, *5*, 13467.
- [31] I. P. Steinke, P. P. Ruden, *J. Appl. Phys.* **2012**, *111*, 014510.
- [32] K. Nomura, T. Kamiya, H. Ohta, K. Ueda, M. Hirano, H. Hosono, *Appl. Phys. Lett.* **2004**, *85*, 1993.
- [33] A. de J. de Meux, G. Pourtois, J. Genoe, P. Heremans, *J. Phys.: Condens. Matter* **2017**, <https://doi.org/10.1088/1361-648X/aa608c>.
- [34] Y. Natsume, H. Sakata, T. Hirayama, H. Yanagida, *J. Appl. Phys.* **1992**, *72*, 4203.
- [35] F. Torricelli, J. R. Meijboom, E. Smits, A. K. Tripathi, M. Ferroni, S. Federici, G. H. Gelinck, L. Colalongo, Z. M. Kovacs-Vajna, D. de Leeuw, E. Cantatore, *IEEE Trans. Electron Devices* **2011**, *58*, 2610.
- [36] R. A. Street, *Hydrogenated Amorphous Silicon*, Cambridge University Press, Cambridge, UK **2005**.
- [37] F. Torricelli, E. C. P. Smits, J. R. Meijboom, A. K. Tripathi, G. H. Gelinck, L. Colalongo, Z. M. Kovacs-Vajna, D. M. De Leeuw, E. Cantatore, *IEEE Trans. Electron Devices* **2011**, *58*, 3025.
- [38] A. Zeumault, V. Subramanian, *Adv. Funct. Mater.* **2016**, *26*, 955.
- [39] F. Zhou, B.-S. Yeh, K. A. Archila, J. F. Wager, *ECS J. Solid State Sci. Technol.* **2014**, *3*, Q3027.
- [40] S. Jeong, J. Moon, *J. Mater. Chem.* **2011**, *22*, 1243.
- [41] B. S. Ong, C. Li, Y. Li, Y. Wu, R. Loutfy, *J. Am. Chem. Soc.* **2007**, *129*, 2750.
- [42] S. Jeong, Y.-G. Ha, J. Moon, A. Facchetti, T. J. Marks, *Adv. Mater.* **2010**, *22*, 1346.
- [43] H. Bong, W. H. Lee, D. Y. Lee, B. J. Kim, J. H. Cho, K. Cho, *Appl. Phys. Lett.* **2010**, *96*, 192115.
- [44] D. J. Goyal, C. Agashe, M. G. Takwale, B. R. Marathe, V. G. Bhide, *J. Mater. Sci.* **1992**, *27*, 4705.
- [45] H. Kaga, Y. Kinemuchi, H. Yilmaz, K. Watari, H. Nakano, H. Nakano, S. Tanaka, A. Makiya, Z. Kato, K. Uematsu, *Acta Mater.* **2007**, *55*, 4753.
- [46] Y. Jung, W. Yang, C. Y. Koo, K. Song, J. Moon, *J. Mater. Chem.* **2012**, *22*, 5390.
- [47] J. Chang, K. L. Chang, C. Chi, J. Zhang, J. Wu, *J. Mater. Chem. C* **2014**, *2*, 5397.